Lunar single-scattering, porosity, and surface-roughness characteristics with SMART-1/AMIE

J. Näränen[1], H. Parviainen[2], K. Muinonen*, 1, 3, J.-L. Josset[4], S. Beauvivre[5], P. Pinet[6], S. Chevrel[6], D. Koschny[7], B. Grieger[8], and B. Foing[7]

[1]*Finnish Geodetic Institute, P.O. box 15, FI-02431 Masala, Finland.*
[2]*Instituto de Astrofísica de Canarias, Calle Vía Láctea, E-38205 La Laguna (Tenerife), Spain.*
[3]*Department of Physics, P.O. box 64, FI-00014 University of Helsinki, Finland.*
[4]*Space Exploration Institute, Case postale 774, CH-2002 Neuchâtel, Switzerland.*
[5]*Micro-cameras & Space Exploration, Puits-Godet 10a, CH-2000 Neuchâtel, Switzerland.*
[6]*Observatoire Midi-Pyrénées/CNRS/Université Toulouse III, 14, Avenue Edouard Belin, 31400 Toulouse, France.*
[7]*ESA, ESTEC/SCI-S, postbus 299, 2200 AG Noordwijk, The Netherlands.*
[8]*ESA, ESAC/SCI-OS, Apdo. de correos 78, 28691 Villanueva de la Cañada, Madrid, Spain.*

We analyze the single-scattering albedo and phase function, local surface roughness and regolith porosity, and the coherent backscattering, single scattering, and shadowing contributions to the opposition effect for specific lunar mare regions imaged by the AMIE camera onboard the ESA SMART-1 spacecraft.

INTRODUCTION

The Moon exhibits an opposition effect [1, 2], that is, a nonlinear increase of disk-integrated brightness with decreasing solar phase angle, the angle between the Sun and the observer as seen from the object. Whereas the opposition effect is a ubiquitous phenomenon for atmosphereless solar-system objects at large, the lunar opposition effect is of particular significance as we can witness the brightness of the full Moon with our own bare eyes. In the opposition night, the Moon is roughly twice as bright as in the nights just before and after the opposition.

The lunar opposition effect lacks a widely accepted physical explanation. It has been traditionally explained by mutual shadowing among regolith particles (sizes of several tens of microns; shadowing mechanism SM) large compared to the wavelength of incident light: the particles hide their own shadows at exact opposition (see [3]). Recently, the coherent-backscattering mechanism (CBM) has been introduced to explain the opposition effect (e.g., [4, 5, 6]). CBM is a multiple-scattering interference mechanism, where reciprocal waves propagating through the same scatterers in opposite directions always interfere constructively in the backward-scattering direction but with varying interference characteristics in other directions.

In what follows, we extract the effects of the stochastic geometry from the SMART-1 AMIE lunar photometry ([7]) and, simultaneously, obtain the volume-element scattering phase function of the lunar regolith locations studied. The volume-element phase function allows us to constrain the physical properties of the regolith particles.

*Corresponding author: Karri Muinonen (karri.muinonen@helsinki.fi)

OBSERVATIONS

We include four different lunar mare regions in our study (Fig. 1). Each of these regions covers several hundreds of square kilometers of lunar surface. When selecting the regions, we have required that they have been imaged by AMIE across a wide range of phase angles (α), including the opposition geometry. The phase-angle range covered in total is 0-109°, with incidence and emergence angles (ι and ϵ) ranging within 7-87° and 0-53°, respectively. Overall, 220 images are used for the present study. The pixel scale varies from 288 m down to 29 m during the extended mission phase ended by the SMART-1 spacecraft crashing into the lunar surface. The dataset represents, to our best knowledge, one of the largest phase-angle coverages of specific lunar regions to date. Off-nadir-pointing observations made of these regions allowed for the extensive phase-angle coverage. The clear (or panchromatic) filter was chosen for the present study as it provides the largest field of view and is currently the best-calibrated channel. Large craters and albedo anomalies were excluded from the analysis.

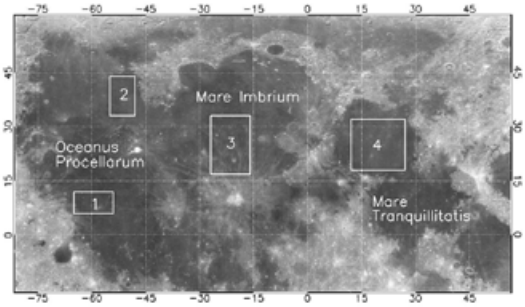

Figure 1. The lunar regions observed by AMIE and analyzed in the present study overlaid on the Clementine albedo map: 1) Oceanus Procellarum, around Reiner Gamma; 2) Oceanus Procellarum, between Mons Rümker and the Mairan crater; 3) Mare Imbrium, north of Copernicus crater; and 4) Mare Serenitatis.

THEORETICAL METHODS

We account for shadowing due to surface roughness and mutual shadowing among the regolith particles with ray-tracing computations for densely packed particulate media with a fractional-Brownian-motion interface with free space. The shadowing modeling allows us to derive the hundred-micron-scale volume-element scattering phase function for the lunar mare regolith. We explain the volume-element phase function by a coherent-backscattering model, where the single scatterers are the submicron-to-micron-scale particle inhomogeneities and/or the smallest particles on the lunar surface. We express the single-scatterer phase function as a sum of three Henyey-Greenstein terms, accounting for increased backward scattering in both narrow and wide angular ranges.

RESULTS AND DISCUSSION

In order to derive the lunar mare volume-element phase function, a best-fit solution to the photometric measurements with phase angles greater than 10° was sought from the computed scattering models using Monte-Carlo minimization techniques. The effects due to different values of packing density v, Hurst exponent H and standard deviation σ in

fractional-Brownian-motion rough surface model were small but noticeable. After the fit, the first-order approximation for the volume-element phase function was obtained by dividing the observational data with the model data (Fig. 2).

The most notable result of the comparison of the photometric measurements and numerical modeling is the inability of SM to explain the intensity surge near the opposition. Even for the most porous media considered in the study, $v = 0.2$, SM cannot explain the behavior of the intensity as a function of decreasing phase angle when $\alpha < 10^\circ$.

The lunar volume-element phase function exhibits a pronounced narrow backscattering enhancement branch that can be assigned to multiple interactions between single scatterers within the volume element. We point out that the related multiple scattering is presently included in what we call the lunar volume-element phase function representing a scattering volume large enough to give rise to coherent-backscattering effects.

In what follows, we present a heuristic scalar coherent-backscattering modeling of the lunar volume-element phase function (see [8]). We fix the radius of the spherical medium at $a = 60$ µm, resulting in a volume roughly equivalent to that of a cubic medium with an edgelength of 100 µm. Fig. 2 shows the best-fit coherent-backscattering model (rms-value of 0.06) with a variation envelope (models with rms-values less than 0.1) among a sequence of models for spherical media of scatterers mimicking the volume element in the lunar surface.

In the modeling, we require that the resulting lunar mare geometric albedos be within $[0.1, 0.2]$ and that the resulting volume-element Bond albedos be within $[0.3, 0.6]$. Such Bond albedos are comparable to the corresponding albedos measured in the laboratory for relevant single particles large compared to the wavelength [9]. The geometric albedos for the mare regions were estimated from the study by [10] and from the characteristics of the AMIE camera.

We obtained acceptable volume-element scattering characteristics using single-scattering albedos $\tilde{\omega} \in [0.7, 0.8]$, extinction mean free paths $k\ell = 60, 90, 120, \ldots, 300$ ($k = 2\pi/\lambda$, where λ is the wavelength), and a triple Henyey-Greenstein single-scattering phase function with total asymmetry parameter $g \approx 0.6$. For the forward and backward-scattering H-G terms, $g_1 = 0.8$ and $g_2 = -0.2$, respectively, with a weight factor of $w_1 = 0.8$ for the former part. For the third H-G term describing narrow backscattering enhancement, $g_3 = -0.9$ with its weight fixed so as to obtain an enhancement by a factor of 1.5 over the value given by the first two H-G terms in the backward-scattering direction.

CONCLUSIONS

Based on the present theoretical modeling of the lunar photometry from SMART-1/AMIE, we conclude that most of the lunar mare opposition effect is caused by coherent backscattering and single scattering within volume elements comparable to lunar particle sizes, with only a small contribution from shadowing effects. We thus suggest that the lunar single scatterers exhibit intensity enhancement towards the backward scattering direction in resemblance to the scattering characteristics experimentally measured and theoretically computed for realistic small particles.

Further interpretations of the lunar volume-element phase function will be the subject of near-future research involving the refinement of the aforedescribed ratioing of the observations and the theoretical model.

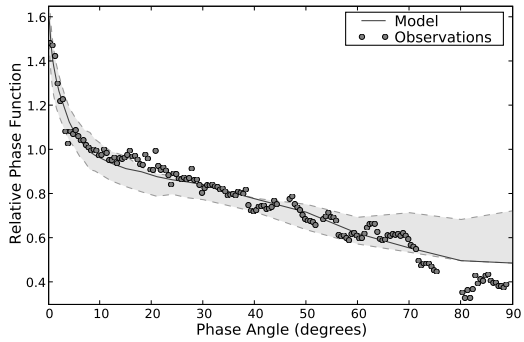

Figure 2. The lunar mare volume-element phase function as obtained from the multiangular AMIE photometry of the mare regions fitted using the fBm-particulate-medium model with $H = 0.4$, $\sigma = 0.06$, and $v = 0.35$ and the corresponding coherent-backscattering modeling. Triple Henyey-Greenstein single-scattering phase functions give rise to coherent-backscattering peaks capable of matching the observations. We show the best-fit coherent-backscattering model as well as a variation envelope resulting from our simulations.

We find that it is possible to derive information about submicron-to-micron-scale surface properties based on multiangular imaging of the target areas. We put forward a novel method where the stochastic surface geometry is derived from the imaging data, whereafter the reduced data allow the derivation of information on the small-scale physical properties.

REFERENCES

[1] N.P. Barabashev. Astron. Nachr **445** (1922).

[2] A. Rougier. Ann, Obs. Strasbourg **205** (1933).

[3] H. Parviainen and K. Muinonen. Bidirectional reflectance of rough particulate media: ray-tracing solution. JQSRT **110** (2009).

[4] Y.G. Shkuratov. Kinematika i Fizika Nebesnykh Tel **4** (1988).

[5] K. Muinonen. Light scattering by inhomogeneous media: backward enchancement and reversal of linear polarization. Ph.D. thesis, University of Helsinki (1990).

[6] M.I. Mishchenko and J.M. Dlugach. Planet. Space Sci. **41** (1993).

[7] P. Pinet, P. Cerroni, J.-L. Josset, S. Beauvivre, S. Chevrel, K. Muinonen, Y. Langevin, M.A. Barucci, M.C. De Sanctis, Y. Shkuratov, V. Shevchenko, P. Plancke, B.A. Hofmann, M. Josset, P. Ehrenfreund, Z. Sodnik, D. Koschny, M. Almeida and B. Foing. The advanced Moon micro-imager experiment (AMIE) on SMART-1: Scientific goals and expected results. Planetary and Space Science **53** (2005).

[8] K. Muinonen, J. Tyynelä, E. Zubko and G. Videen. Coherent backscattering in planetary regoliths. Light Scattering Reviews (in press) (2010).

[9] J. Piironen, K. Muinonen, T. Nousiainen, C. Sasse, S. Roth and J.I. Peltoniemi. Albedo measurements on meteorite particles. Planetary and Space Science **46** (1998).

[10] K. Lumme and W.M. Irvine. AJ **87** (1982).